

Areg Noshadi*, Michael Kircher, Stefan Pollnow, Gunnar Elke, Inéz Frerichs and Olaf Dössel

Automatic lung segmentation in the presence of alveolar collapse

Abstract: Lung ventilation and perfusion analyses using chest imaging methods require a correct segmentation of the lung to offer anatomical landmarks for the physiological data. An automatic segmentation approach simplifies and accelerates the analysis. However, the segmentation of the lungs has shown to be difficult if collapsed areas are present that tend to share similar gray values with surrounding non-pulmonary tissue. Our goal was to develop an automatic segmentation algorithm that is able to approximate dorsal lung boundaries even if alveolar collapse is present in the dependent lung areas adjacent to the pleura. Computed tomography data acquired in five supine pigs with injured lungs were used for this purpose. First, healthy lung tissue was segmented using a standard 3D region growing algorithm. Further, the bones in the chest wall surrounding the lungs were segmented to find the contact points of ribs and pleura. Artificial boundaries of the dorsal lung were set by spline interpolation through these contact points. Segmentation masks of the entire lung including the collapsed regions were created by combining the splines with the segmentation masks of the healthy lung tissue through multiple morphological operations. The automatically segmented images were then evaluated by comparing them to manual segmentations and determining the Dice similarity coefficients (DSC) as a similarity measure. The developed method was able to accurately segment the lungs including the collapsed regions (DSCs over 0.96).

Keywords: image processing, lung segmentation, alveolar collapse.

<https://doi.org/10.1515/cdbme-2017-0188>

*Corresponding author: **Areg Noshadi:** Institute of Biomedical Engineering, Karlsruhe Institute of Technology (KIT), Kaiserstr. 12, 76128 Karlsruhe, Germany, e-mail: publications@ibt.kit.edu

Michael Kircher, Stefan Pollnow, Olaf Dössel: Institute of Biomedical Engineering, Karlsruhe Institute of Technology (KIT), Kaiserstr. 12, 76128 Karlsruhe, Germany, e-mail: publications@ibt.kit.edu

Gunnar Elke, Inéz Frerichs: Department of Anaesthesiology and Intensive Care Medicine, University Medical Centre Schleswig-Holstein, Campus Kiel, Arnold-Heller-Strasse 3 Haus 12, 24105 Kiel, Germany, e-mail: Gunnar.Elke@uksh.de, Inez.Frerichs@uksh.de

1 Introduction

Lung ventilation and perfusion analyses using chest imaging methods require an anatomically correct segmentation of the organ. In clinical practice, computed tomography (CT) scans are performed for this purpose and the acquired images need to be manually segmented to offer anatomical landmarks for the physiological data. Due to the large amount of imaging data, an automatic segmentation approach simplifies and accelerates the analysis. However, the segmentation of the lungs has shown to be difficult if collapsed areas are present that tend to share similar gray values with surrounding non-pulmonary tissue. Existing automatic segmentation algorithms for healthy lungs are not precise in the presence of lesions near the pleura [1]. We present an automatic segmentation approach that is able to approximate dorsal lung boundaries even if alveolar collapse is present in the dependent lung areas adjacent to the pleura. To develop the segmentation algorithm, we used CT data acquired in pigs with regionally injured lungs from an experimental study [2] where the data were used as reference for lung ventilation and perfusion measurements with electrical impedance tomography (EIT).

2 Methods

The study from which the CT data was gathered was approved by the University of Iowa committee for animal care and adhered to the guidelines on animal experimentation. Regional

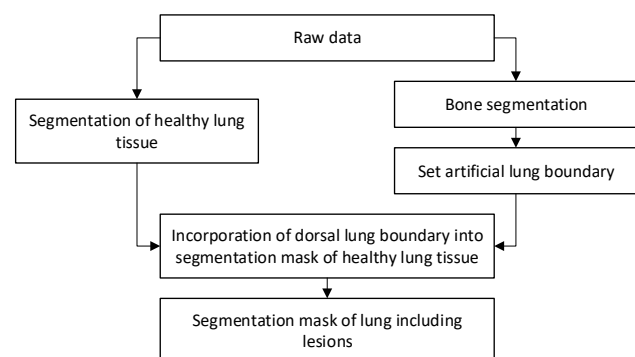


Figure 1: Processing steps of the segmentation approach.

lung injury was induced in two adjacent sublobar segments of the right lung by repetitive saline lavage or endotoxin injury. MathWorks MATLAB R2016b software was used for the implementation of the automatic segmentation algorithm. The given CT data sets (DICOM format) of five supine pig thoraces consisted of slices with resolutions of 512×512 pixels and slice numbers of approx. 600 (slice thickness = 0.75 mm). Figure 1 shows the multiple processing steps of the segmentation approach. The complete segmentation mask was created by combining the segmentation results of the healthy lung area (obtained through 3D region growing (RG) with automatic seed point selection) and the dorsal lung boundary. The latter had to be calculated using a spline interpolation by segmenting the bones surrounding the lungs and then finding the contact points of rib cage and pleura.

2.1 Bone segmentation

Bone segments in the chest wall were segmented for determining the contact points of bones and pleura. First, a global threshold was applied. 3D RG had to be performed for segmenting the ribcage including the spine at once. However, contrast medium in the heart and vessels had similar gray values as bones and was sometimes touching ventral bones (especially the sternum), hence additional processing steps had to be inserted to remove the unwanted pixels:

A parabola was calculated which contained the upper corner pixels of the image ($P_1 = (0|0)$, $P_2 = (x_{max}|0)$). The apex of the parabola was chosen as $P_3 = (\frac{x_{max}}{2}|C_{healthy,y})$ with $C_{healthy,y}$ as the y-coordinate of the previously segmented healthy lung area centroid $C_{healthy}$ (see Figure 2). All white pixels above the parabola were set to 0 (black). Before starting the 3D RG, morphological closing was performed in order to close small gaps between vertebra and rib segments. This ensured that all ribs were segmented during RG with a single seed point selection. Finally, the seed point for 3D RG was selected automatically as a random pixel from the largest bone region.

2.2 Approximation of dorsal lung boundary

The contact points of bones and pleura were determined through the following steps:

The centroid of the entire segmented healthy lung tissue region in a slice $C_{healthy}$ and the centroids of each of the i regions in the segmented bone image $C_{bone,i}$ were located. For each of the j bone regions that had a significant size (threshold = 20% of mean region area), a pixel-value cross-section vector $\mathbf{g}_{cs,j}$ was created, which consisted of all pixel values in

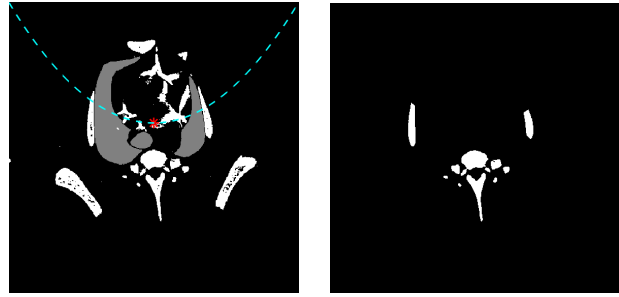


Figure 2: Thresholded image (white) with parabola through P_3 (dotted line). The previously segmented healthy lung tissue is visualized in gray (left). Final bone segmentation result (right).

the bone image along the line connecting $C_{healthy}$ and $C_{bone,i}$. Each $\mathbf{g}_{cs,j}$ was searched for the first nonzero element (starting at $C_{healthy}$). These pixels were saved as contact points of bone and pleura (see Figure 3 (a)). In many cases, the region area from the spinous process was exceeding the 20% threshold. In these cases, $\mathbf{g}_{cs,j}$ was crossing the vertebra region and the first nonzero element found was on the vertebra.

Depending on the bone region constellation in a slice, the deviation of the spline from the pleura would be high, if the distance between neighboring dorsal bone segments was too large. Thus, all previously found contact points from slice $n-15$ to $n+15$ were added to slice n (see Figure 3 (b)). It was assumed that the shape of the dorsal lung boundary did not significantly change within this range of 31 slices (total thickness of 22.5 mm). However, the bone segments changed their position far enough to obtain a sufficient amount of extra contact points between two neighboring bone regions with large distance.

The points were divided into two sets: P_n contained points found in slice n , the remaining points (found on slice $n-15$ to $n+15$ and later added to slice n) were included in P_r . In a next step, redundant points were excluded to improve the smoothness of the spline. The exclusion was carried out considering following criteria (see Figure 3 (c)):

Points within bone regions of slice n (surrounded by white pixels only) were dismissed. If two points from P_n were too close to each other (distance $< d_1$), the one with the larger distance to $C_{healthy}$ was dismissed. Points from P_r too close to points from P_n were removed (distance $< d_2$). If two points from P_r were too close to each other (distance $< d_3$), the one with the larger distance to $C_{healthy}$ was removed.

The distances d_1 , d_2 and d_3 were chosen via empirical analysis. Points out of P_n had the least deviation from the real lung boundary. Therefore, d_2 was set relatively high, since points from other slices (P_r) would only falsify the boundary in the environment of points from P_n . d_1 and d_3 were chosen relatively small values as the points were not necessarily deviating

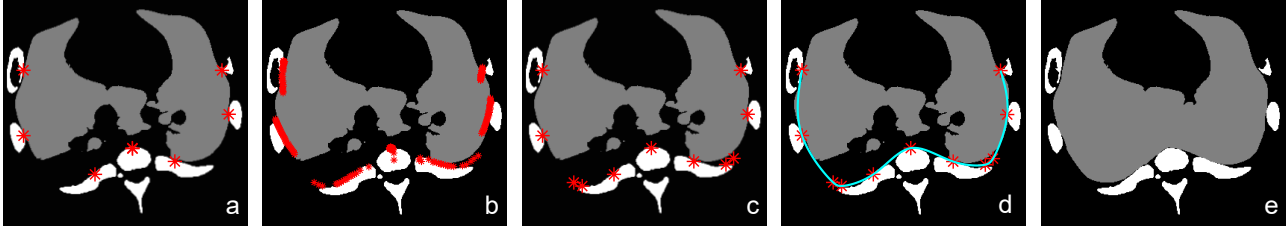


Figure 3: (a): Bone and Pleura contact points. (b): Additionally added contact points. (c): Contact point after redundant points were removed. (d): Spline interpolation through given contact points. (e): Final segmentation mask including collapsed regions.

significantly from the boundary within this distance, but points that close were counterproductive for the smoothness of the spline.

Finally, a natural cubic spline was set through the k given contact points $P_{contact,k}$ (see Figure 3 (d)). The MATLAB function *cscvn* was used to create a natural cubic spline through $P_{contact,k}$. This function uses E. Lee’s centripetal scheme [3] to chose the parameter value $t(k)$ for the k th point.

2.3 Segmentation mask

Finally, the segmentation masks of the healthy lung tissue had to be combined with the obtained splines to receive segmentation masks for the whole lung including collapsed areas. With the segmentation mask of healthy lung tissue as the initial image, this was achieved as follows: Morphological closing was performed to close small interruptions in the healthy lung tissue regions. Pixel values along the spline were set to 1 (white). Horizontal and vertical rows of white pixels were set through the centroid of the healthy lung tissue region to guarantee that performing morphological filling in the next step would fill the gap between the spline and the segmentation mask of the healthy lung tissue. After filling, morphological opening was performed to remove the excess spline and lines outside the lung region. Bone regions of the previous five and upcoming 15 slices (slice numbers increasing in caudal direction) were subtracted, then the image matrix was thresholded for values ≥ 0 . This removed excess parts of the segmentation mask caused by the spline reaching far outside the lungs. The unsymmetrical selection of the slice numbers to subtract the bone regions was due to the shape of the bone regions and their outwards movement with increasing slice numbers. Finally, morphological opening was performed to smooth the dorsal edge of the mask (see Figure 3 (e)).

3 Results

The automatic segmentation algorithm was tested on data sets from five different swines. Animal 1, 3, 5 and 9 included

lavage injury, animal 4 included endotoxin injury [2]. Manual segmentations performed by physicians were available for a varying number of slices around the EIT belt level of each data set. These were used as reference segmentations to evaluate the results of the automatic algorithm. Three slices of each animal were considered for the comparison since this was the highest number of available reference segmentations for every animal.

The Dice similarity coefficient (DSC) was used as a similarity measure to determine the accuracy of the segmentations [4]. With A_a as the area of the segmentation mask from the automatic algorithm, A_{ref} as the area of the reference manual segmentation by the physician and $A_a \cap A_{ref}$ as the overlapping area of the two segmentation masks, the DSC was calculated as:

$$DSC(A_a, A_{ref}) = \frac{2(A_a \cap A_{ref})}{A_a + A_{ref}} \quad (1)$$

The DSCs were calculated for the entire segmentation masks and for their quadrants (numbering goes counter-clockwise starting from the upper right quadrant) to obtain additional information about the similarity in different image regions (see Table 1). Figure 4 shows a comparison of an automatically segmented slice and its manually segmented reference.

	Dice similarity coefficients				
	Total	Quadrant			
		I	II	III	IV
Animal 1	0.9805	0.9857	0.9800	0.9785	0.9778
Animal 2	0.9771	0.9795	0.9855	0.9651	0.9790
Animal 3	0.9685	0.9646	0.9562	0.9737	0.9778
Animal 4	0.9773	0.9770	0.9743	0.9757	0.9820
Animal 5	0.9830	0.9801	0.9857	0.9787	0.9867
μ	0.9758	0.9694	0.9739	0.9770	0.9818
σ	0.0050	0.0101	0.0122	0.0070	0.0043

Table 1: DSCs of automatic and manual reference segmentation for the total segmentation mask and their quadrants masks for the five studied animals (one example slice per animal). Means μ and standard deviations σ of all DSCs determined in the study.

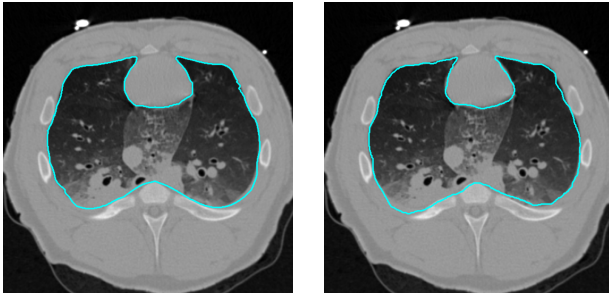


Figure 4: Automatic segmentation result (left) and manually segmented reference (right) of Animal 2. $DSC_{total} = 0.9771$

4 Discussion

The developed method proved to deliver solid results for the parts of the lungs where manually segmented reference images were available (mediastinum was included). Automatic segmentations of the selected slices were very similar to the manual reference segmentations with the total DSCs always higher than 0.96. It is noticeable that the mean DSCs of quadrant III and IV and their variance were higher than the other two. Considering that the ventral lung boundary was found by RG, this seems to be contradictory at first. The ventral lungs did not contain many lesions in our data, hence the lungs had a clear ventral boundary with a clearly visible gray value difference. This outcome was due to two reasons:

The perimeters of the segmentations masks deviated in the heart region. The automatic algorithm detected the darker part of the heart as lung boundary, the gray value fell below the threshold. Further, the manual segmentations were not precise in those regions. These parts with distinct gray value differences will always be detected more accurately with RG. Nevertheless, the manual segmentations had to be regarded as the ground truth since no other reference was available.

The reference segmentations originated from caudal regions of the lungs. These parts of the thorax were captured by EIT and CT in the study by Elke et al. [2]. Particularly in these regions of the lungs the automatic algorithm performed best. Moving up to the apex of the lungs, the algorithm became inaccurate or failed totally. The bone segments did not provide suitable interpolation points as the ribcage got narrower. Problems appeared if extensive lesions were in the ventral regions of the lungs as the ventral boundary was found by RG only.

The algorithm either requires baseline scans or a data set of larger parts of the lung. It can not be performed on single slices since 3D segmentation algorithms are used and the spline calculation of each slice relies on information of subsequent slices.

Mesanovic et al. introduced an automatic algorithm for lung segmentation which worked imprecisely if lesions were attached to the pleura [1]. This is comparable to the lesion distribution in our data set. Xin et al. developed a semi-automatic registration-based multilandmark method [5] which needed previously (in their case manually) segmented references of healthy lungs. In contrast, our developed algorithm does not need any comparative references (segmentations of the healthy lungs), it works automatically with the data sets of the injured lungs.

Author's Statement: Research funding: S. Pollnow is supported by a scholarship of the Karlsruhe School of Optics and Photonics. Conflict of interest: Authors state no conflict of interest. Informed consent: Informed consent is not applicable. Ethical approval: The study from which the CT data was gathered was approved by the University of Iowa committee for animal care and adhered to the guidelines on animal experimentation.

References

- [1] Mesanovic N, Grgic M, Huseinagic H, Males M, Skejic E, Smajlovic M. Automatic CT image segmentation of the lungs with region growing algorithm. 18th International Conference on Systems, Signals and Image Processing-IWSSIP 2011; 395–400.
- [2] Elke G, Fuld MK, Halawish AF, et al. Quantification of ventilation distribution in regional lung injury by electrical impedance tomography and xenon computed tomography. *Physiological measurement* 2013; 34(10): 1303–1318.
- [3] Lee ETY, Choosing nodes in parametric curve interpolation. *Computer-Aided Design* 1989; 21(6): 363–370.
- [4] Zou KH, Warfield SK, Bharatha A et al. Statistical validation of image segmentation quality based on a spatial overlap index 1: Scientific reports. *Academic radiology* 2004; 11(2): 178–189.
- [5] Xin Y, Song G, Cereda M et al. Semiautomatic segmentation of longitudinal computed tomography images in a rat model of lung injury by surfactant depletion. *Journal of Applied Physiology* 2015. 118(3): 377–385.